Prepared for submission to Wiley

AUSM-like Expression of HLLC and Its All-Speed Extension

Keiichi Kitamura [a, *] and Eiji Shima [b]

a) Yokohama National University, 79-5 Tokiwadai, Hodogaya-ku, Yokohama, Kanagawa 240-8501, Japan

b) Japan Aerospace Exploration Agency (JAXA), 3-1-1 Yoshinodai, Sagamihara, Kanagawa 252-5210, Japan

Abstract

AUSM (Advection-Upstream-Splitting-Method) and HLLC (Harten-Lax-van_Leer with Contact) are two popular families of flux functions. The AUSM is simple and requires no eigenstructure, which facilitates its extensions to general equations-of-state. Furthermore, one of its variants, SLAU (Simple Low-dissipation AUSM) (Shima and Kitamura, 2011, AIAA Journal) is applicable to all speeds and features removal of parameter-setting by the user. HLLC, on the other hand, clearly defines three distinct waves in Riemann problem, namely, left-running and right-running acoustic waves, and entropy wave. This note demonstrates that HLLC can be written in a very similar form with the AUSM family, and that the similar manner in extending AUSM family to all speeds is easily incorporated into HLLC in this AUSM-like form. Then, we combine the strengths of the both flux functions, and offers a new inviscid numerical flux function within the framework of MUSCL (Monotone Upwind Scheme for Conservation Laws) in CFD (Computational Fluid Dynamics) for Euler and Navier-Stokes equations. The resultant, HLLCL (HLLC with Low-dissipation) numerical flux can compute low Mach number flows and sound propagations at the same time with high accuracy, as demonstrated by one-dimensional and two-dimensional numerical examples. Furthermore, the results indicate that its extensions to general fluids such as supercritical fluids are encouraging.

Keywords: HLLC; AUSM; SLAU; HLLCL; Finite Volume Method; All Speeds

[*] corresponding author; tel: +81-45-339-3876, e-mail address: kitamura@ynu.ac.jp

1. Introduction

MUSCL (Monotone Upwind Scheme for Conservation Laws) [1] type schemes have been applied for many practical CFD (Computational Fluid Dynamics) computations and are the basis of modern CFD algorithms. Numerical flux functions that calculate an inviscid flux at computational cell boundaries are one of the crucial points in this framework. This note presents a new inviscid numerical flux scheme for MUSCL in CFD for Euler and Navier-Stokes equations to compute low Mach number flows and sound propagations at the same time with high accuracy, based on HLLC (Harten-Lax-van_Leer with Contact) scheme [2].

It has been known that the inviscid numerical flux can be formulated in a simple and robust manner by AUSM (Advection Upstream Splitting Method) family schemes [3, 4, 5]. The authors proposed all-speed flux functions based on AUSM family schemes, named SLAU (Simple Low-dissipative AUSM) [6], SLAU2 [7] and SD (Shock Detecting)-SLAU [8], which have been successfully applied to various low Mach number flows. These schemes can compute low Mach number flows and sound in these (perfect-gas) flows at the same time. Such features are favorable to compute low Mach number flows directly coupled to the sound. For aerospace applications, however, combustion instabilities in a liquid rocket engine and flows in sound resonators are typical examples [9] in which the perfect gas assumption is too crude.

Here let us mention flows in the combustion chamber of the liquid rocket engine into which cryogenic oxygen and sometimes gaseous hydrogen are injected. Typically, they are turbulently mixed, vaporized and burned. In certain cases, a standing wave in the chamber interacts with the combustion, then the oscillating combustion or the combustion instability occurs [9]. Therefore, we have to treat two phases (liquid and gas) expressed by different equations-of-state (EOSs), turbulent mixing, combustion and so on. All of these are very tough problems and could not be resolved easily by one single technology. We will propose, however, a new methodology that can handle general EOSs of two-phase flows and potentially alter the existing numerical analysis.

Although it is also possible to treat general EOSs in AUSM family schemes, we have to admit that the AUSM family contains ambiguity in describing both sides of the Riemann problem as in the flux vector splitting (FVS) scheme [10], that is, we are unable to predict which side of fluids will flow into the other *a priori*, without the help of Godunov [27] or HLLC solver [28], in the context of two-fluid modeling (Kim et al. [31, 32] successfully extended AUSM family schemes to multiphase flows by one-fluid modeling (or homogeneous mixture modeling), in which pressure and velocity equilibriums are assumed between phases). On the other hand, multiphase flows of

general EOSs can be more naturally treated by HLLC scheme [2] since the numerical flux is clearly defined from conservation laws by only determining three wave speeds: HLLC defines three distinct waves in the Riemann problem, namely, left-running and right-running acoustic waves (s_L and s_R), and an entropy wave, $s*$ (Fig. 1). In this example (Fig. 1), it is clearly seen that the left side fluid (e.g., water in the "L" region) will be conveyed to the cell-interface (e.g., "*L" region), not the fluid from the right side fluid (e.g., air in the "R" region). This is one of strengths of HLLC. Therefore, we intend to use HLLC as the basis of a new all-speed scheme by combining its accuracy with the simplicity of the AUSM family.

An extension of HLLC (or the similar numerical flux) to all speeds is not new. In their extension, Luo et al. [11] scaled not only the acoustic speed but also the convective velocity by borrowing a parameter from a pre-conditioner. Park et al. [12] employed the similar idea to HLLE+ scheme. While they were successful in solving aerodynamic problems, their applicability to aero-acoustic problems had not been discussed, in contrast with the present work. This paper will offer an alternative formulation of HLLC for all speeds (HLLC with Low-dissipation, HLLCL) covering both aerodynamic and aero-acoustic simulations. Furthermore, as in SLAU [6], the present extension of HLLC to all speeds is based on i) *a simpler and more flexible formulation* free from an eigenmatrix structure, and ii) *a robust, multidimensional velocity* consideration, in contrast with the classical, time-derivative-preconditioning-based formulation [13]. We emphasize that it is not our current scope to demonstrate superiorities of HLLCL over the existing methods such as SLAU at all flow speeds, in every numerical test. Instead, we will pursue a new method that can be used for both a variety of flows (e.g., low speeds) and acoustic simulations. We hope that the newly-proposed HLLCL will also serve as a bridge between HLLC and AUSM families, and further promote their extensions to general fluids such as multiphase flows or supercritical fluids [one example for supercritical Nitrogen, governed by Soave-Redlich-Kwon (SRK) EOS [24], will be shown in Appendix]. Folkner et al. [33] and Kim et al. [31, 32] applied an unsteady preconditioning technique to Convective-Upwind Split-Pressure (CUSP) and AUSM family schemes for very low Mach number unsteady flows. In contrast with such a technique, the present method will not require Strouhal number setting.

This paper is constructed as follows. In Section 2, the governing equations and HLLC scheme in the AUSM-like form are introduced. Then, an "embedded" numerical dissipation of HLLC is theoretically analyzed and the new scheme will be proposed. Numerical examples of basic 1-D and 2-D problems including low Mach number flows and sound propagations are shown in Section 3. Section 4 concludes the present work.

2. Governing Equations and Formulations

2.1 Finite Volume Formulation and AUSM family numerical flux scheme

The governing equations are the compressible Navier-Stokes equations, written in the integral form as follows:

$$\iiint \mathbf{Q}_t \, dv + \oiint (\hat{\mathbf{E}} - \hat{\mathbf{R}}) ds = 0 \tag{1}$$

Here $\mathbf{Q}$, $\hat{\mathbf{E}}$, and $\hat{\mathbf{R}}$ are vectors of conservative variable, inviscid and viscous fluxes at the cell-interface, respectively. By applying the equation to a polyhedral computational cell, the basic form of a finite volume method (FVM), which is common to both structured and unstructured meshes, is obtained as

$$\frac{\mathbf{Q}^{n+1}{}_i - \mathbf{Q}^n{}_i}{\Delta t} + \frac{1}{\Omega_i} \sum_j (\tilde{\mathbf{E}}_{i,j} - \tilde{\mathbf{R}}_{i,j}) S_{i,j} = 0 \tag{2}$$

Here $\tilde{\mathbf{E}}_{i,j}$ and $\tilde{\mathbf{R}}_{i,j}$ are numerical inviscid and viscous fluxes at the cell-interface respectively, Ω_i is the cell volume, Δt is the time step, and $S_{i,j}$ is the interfacial-area separating cells i and j. Since the viscous term is treated in a conventional manner, we will focus on the inviscid flux here.

It had been shown that the inviscid numerical flux function can be formulated as simple and robust as in AUSM family schemes. The authors have demonstrated that we can derive all-speed flux schemes by modifying the numerical dissipation in the AUSM family scheme [6]. We will follow the similar way to improve HLLC.

The numerical flux function of an AUSM family scheme is written as

$$\tilde{E}_{AUSM} = \frac{\dot{m} + |\dot{m}|}{2} \mathbf{\Phi}_L + \frac{\dot{m} - |\dot{m}|}{2} \mathbf{\Phi}_R + \tilde{p}\mathbf{N} \tag{3a}$$

$$\mathbf{\Phi} = (1, u, v, w, h)^T \tag{3b}$$

$$\mathbf{N} = (0, x_n, y_n, z_n, 0)^T \tag{3c}$$

$$h = (e + p)/\rho \tag{3d}$$

Here u, v, w, h, e, p, ρ, and $\mathbf{N}$ are velocity components in x, y, z directions, total enthalpy, total energy (per unit volume), pressure, density, and a unit outward normal vector at the cell interface, respectively, and values with subscript "L" or "R" indicate reconstructed values at the cell interface in MUSCL type CFD algorithms. In addition, $\dot{m}$ and $\tilde{p}$ denote the mass flux and the numerical pressure at the cell-interface, and variations of them have yielded

variants within AUSM family schemes. The formulation of the numerical pressure was inherited from van Leer's FVS method [10] and the authors have shown that this term also works as numerical dissipation that stabilizes computations. In addition, it was also shown that the amount of this numerical dissipation should be properly scaled for accurate low-dissipation computations of low Mach number flows.

2.2 HLLC scheme and its AUSM-like expression

Harten, Lax and van Leer [14] reported the way to determine the inviscid flux function by solving the approximate Riemann initial value problem. There are three characteristic speeds in the inviscid fluid, i.e., left- and right-running acoustic waves, s_L, s_R, and one convective speed, s_* (Fig. 1). Assuming two constant intermediate states divided by three discontinuities, they showed that the numerical flux is uniquely defined to reproduce integrated values at both sides in which the above-mentioned wave structure exists†.

Toro et al. [2] showed in their development of HLLC scheme that contact surfaces and boundary layers are correctly captured when the characteristic speed corresponding to the convective speed s_* is properly given. If the three wave speeds are provided (Fig. 1), the interface flux is obtained automatically without the need for computing the Jacobian of the flux, and therefore, HLLC scheme can be easily applied to the general EOSs (with no ambiguity). Note that although the three wave speeds mimic the physical waves, we can modify those wave speeds and alter the characteristics of the scheme in numerical algorithms [15].

Let us now try to *express HLLC scheme* [2] *in an AUSM-like form* as follows

$$\widetilde{E}_{HLLC} = \frac{\dot{m}+|\dot{m}|}{2}\boldsymbol{\Phi}'_L + \frac{\dot{m}-|\dot{m}|}{2}\boldsymbol{\Phi}'_R + \widetilde{p}\mathbf{N} \tag{4a}$$

$$\boldsymbol{\Phi}'_{L/R} = \boldsymbol{\Phi}_{L/R} + \begin{pmatrix} 0 & 0 & 0 & 0 & \dfrac{\widetilde{s}_{L/R}\left(p_* - p_{L/R}\right)}{\rho_{L/R}\left(s_{L/R} - V_{L/R}\right)} \end{pmatrix}^T \tag{4b}$$

Here $\widetilde{s}$ denotes the (numerical) characteristic speed (to be defined later). This expression helps us to understand (and even change) the numerical dissipation of HLLC scheme. Although the energy term is slightly different, HLLC scheme appears to have the similar form to the AUSM family schemes. Then, the mass flux and the numerical pressure of HLLC are expressed as

† There may be some confusions regarding HLL Riemann solvers, but the original HLL consists of two variants: two-wave and three-wave HLL [13] (as claimed by Prof. Bram van Leer himself at "Four Decades of CFD: Looking Back and Moving Forward - A symposium celebrating the careers of Jameson, Roe and van Leer (JRV Symposium)," June 23, 2013, http://dept.ku.edu/~cfdku/JRV.html), although the former is more widely recognized as the 'original' HLL having no contact-resolving capability.

$$\dot{m} = \begin{cases} \rho_L V_L + \tilde{s}_L(\rho_{L*} - \rho_L) & s_* > 0 \\ \rho_R V_R + \tilde{s}_R(\rho_{R*} - \rho_R) & otherwise \end{cases} \tag{5a}$$

$$\tilde{p} = p_* + \begin{cases} \dfrac{s_*}{s_* - \tilde{s}_L}(p_L - p_*) & s_* > 0 \\ \dfrac{s_*}{s_* - \tilde{s}_R}(p_R - p_*) & otherwise \end{cases} \tag{5b}$$

$$\rho_{L/R*} = \frac{s_{L/R} - V_{L/R}}{s_{L/R} - s_*}\rho_{L/R} \tag{5c}$$

$$\tilde{s}_L = \min(0, s_L), \quad \tilde{s}_R = \max(0, s_R) \tag{5d}$$

$$\alpha_L = \rho_L(V_L - s_L) > 0, \quad \alpha_R = \rho_R(s_R - V_R) > 0 \tag{5e}$$

$$V = x_n u + y_n v + z_n w \tag{5f}$$

$$p_* = \frac{1}{2}\{p_L + p_R + \alpha_L(V_L - s_*) - \alpha_R(V_R - s_*)\} \tag{5g}$$

where * is referred to as a "star region," located between the left (L) and right (R) states, as seen in Fig. 1. The definition of the numerical flux will be completed when the three characteristic speeds, i.e., s_L, s_R and s_*, are given. We will keep this framework throughout this research. Now many ideas that have already been applied so far to improve AUSM family schemes are expected to be easily introduced to HLLC scheme from this AUSM-like notation. Note that Liou [29] expressed HLLE (Harten-Lax-van_Leer-Einfeldt) flux (a two-wave solver) [23] in the AUSM like form. However, HLLE flux does not give correct behavior at contact discontinuities [29] and the resolution of low Mach number flows was not considered in his expression as in the original HLLE scheme. Thus, its resolution is expected to be poorer than all-speed AUSM family schemes such as SLAU[6], because the convective speed s_*, which plays a crucial role in low Mach number flows, is ignored as in the original HLLE.

2.3 Analysis of the "embedded" numerical dissipation of HLLC (1): Interface pressure

From the Eq.(5b), it is clear that the interface pressure consists of two parts: p_* and the second part containing p_L or p_R. It is also seen that the second part works so as to turn the interface pressure completely upwinded at

supersonic condition, where $\tilde{s}_L = 0$ or $\tilde{s}_R = 0$. Therefore, the second term can be regarded as an upwind switch for the pressure term.

In order to see how p_* works at low speeds, on the other hand, we rewrite the first term as

$$p_* = \frac{1}{2}\left\{ p_L + p_R + \frac{\rho_L \tilde{c}_L + \rho_R \tilde{c}_R}{2}(V_L - V_R) + \frac{\rho_L \tilde{c}_L - \rho_R \tilde{c}_R}{2}(V_L + V_R - 2s_*) \right\} \tag{6a}$$

Here the following notations are used;

$$s_L = V_L - \tilde{c}_L, \quad s_R = V_R + \tilde{c}_R \tag{6b}$$

where $\tilde{c}_L$ and $\tilde{c}_R$ are numerical sound speeds that are not necessarily the physical ones. Then, we assume here as

$$\tilde{c}_L = \tilde{c}_R \equiv \tilde{c}_1 \tag{7a}$$

$$\rho_L = \rho_R \equiv \rho_1 \tag{7b}$$

Then, from Eq.(6a),

$$p_* = \frac{1}{2}\left\{ p_L + p_R - \rho_1 \tilde{c}_1 (V_R - V_L) \right\} \tag{8}$$

Therefore, it is seen that p_* consists of the average of pressures of both sides and the "embedded" numerical dissipation, whose amount is determined by the scale of $\tilde{c}_1$. The dissipation given by the sound speed is of an appropriate scale for high Mach number flows; however, it will be too large for low Mach number flows [6, 13]. There is a similar mechanism in the pressure term of AUSM family schemes [5, 6].

2.4 Analysis of the embedded numerical dissipation of HLLC (2): Mass flux

Batten et al. [15] proposed the definition of s_* as

$$\left(s_*\right)_{Batten} = \frac{\alpha_L V_L + \alpha_R V_R - \Delta p}{\alpha_L + \alpha_R} \tag{9}$$

here 'Δ' denotes difference of both sides such as

$$\Delta p = p_R - p_L \tag{10}$$

By assuming s_*>0, $s_L = V_L - \tilde{c}_L$ <0 and $s_R = V_R + \tilde{c}_R > 0$, substitution of Eq.(9) to Eqs.(5a,5c) makes the mass flux

$$\dot{m} = \frac{\rho_L \tilde{c}_L \left(\rho_L \tilde{c}_L V_L + \rho_R \tilde{c}_R V_R - \Delta p \right)}{\rho_L \tilde{c}_L{}^2 + \rho_R \tilde{c}_R \left(V_R - V_L + \tilde{c}_L \right) - \Delta p} \tag{11}$$

Furthermore, assuming $\tilde{c}_L$ and $\tilde{c}_R$ are constants, the first order Taylor expansion centered at ($\overline{\rho}, \overline{V}, \overline{p}$) about $\Delta\rho$, ΔV and Δp leads to the following approximate expression for the mass flux

$$\dot{m} \approx \overline{\rho}\overline{V} - \frac{1}{2}\overline{V}\Delta\rho + \overline{\rho}\frac{\tilde{c}_L\left(\tilde{c}_R - \tilde{c}_L\right) + 2c_R\overline{V}}{4\tilde{c}_L\overline{\tilde{c}}}\Delta V - \frac{1}{2\overline{\tilde{c}}}\left(1 - \frac{\overline{V}}{\tilde{c}_L}\right)\Delta p \tag{12}$$

where the values with a bar denote the arithmetic averaged values. On the other hand, the mass flux of Roe scheme can be written for subsonic flows as

$$\dot{m}_{Roe} = \frac{(\rho V)_L + (\rho V)_R}{2} - \frac{1}{2}\left|\overline{V}\right|\Delta\rho - \overline{\rho}\frac{\overline{V}}{2\overline{c}}\Delta V_n - \frac{1}{2\overline{c}}\left(1 - \frac{\left|\overline{V}\right|}{\overline{c}}\right)\Delta p \tag{13}$$

Note that the Roe scheme gives linearized solution of the Riemann initial value problem (R.I.P.) of the Euler equation and that averages in Roe scheme are evaluated by the Roe average. It is obvious that Eq.(12) and Eq.(13) give almost the identical flux if $\tilde{c}_L = \tilde{c}_R$ in Eq.(12) and $\overline{V}$ >0 in Eq.(13), therefore, Eq.(12) also gives the linearized solution of R.I.P. Furthermore, both of them contain the pressure difference term (last term) which had been found essential to stabilize low Mach number flows [6].

2.5 Proposal of new flux scheme: HLLCL (HLLC with Low-dissipation)

It is shown in 2.4 that the interface pressure contains the embedded numerical dissipation and that their scale should be reduced for low Mach number flows. Now let us briefly introduce an example of *conventional* scaling for low speeds (not employed here). Luo et al. [11] showed that all characteristic speeds can be scaled to the convective velocity order using numerical characteristic speeds derived from the time derivative pre-conditioning method. If the time derivative pre-conditioning method of Weiss and Smith [13] is applied, numerical signal speeds are expressed as

$$\begin{aligned} \left(s_L\right)_{Luo} &= \frac{1}{2}\left\{(1+\varepsilon^2)V_L - \sqrt{(\varepsilon^2-1)^2 V_L{}^2 + 4\varepsilon^2 c_L^2}\right\}, \\ \left(s_R\right)_{Luo} &= \frac{1}{2}\left\{(1+\varepsilon^2)V_R + \sqrt{(\varepsilon^2-1)^2 V_R{}^2 + 4\varepsilon^2 c_R^2}\right\} \end{aligned} \tag{14}$$

where ε is a non-dimensional parameter that has a scale of the convective Mach number. For this case, numerical speeds of sound can be expressed as;

$$\begin{aligned}\tilde{c}_L &= \frac{c_L}{2}\left\{(1-\varepsilon^2)M_L + \sqrt{(1-\varepsilon^2)^2 M_L{}^2 + 4\varepsilon^2}\right\} \\ \tilde{c}_R &= \frac{c_R}{2}\left\{(1-\varepsilon^2)M_R + \sqrt{(1-\varepsilon^2)^2 M_R{}^2 + 4\varepsilon^2}\right\}\end{aligned} \tag{15}$$

Thus, the speed of sound is approximately scaled to the convective speed. In this flux function, if the common density on the both sides and the definition of s_* of Eq.(9) are introduced, the pressure in the star region p_* reduces to;

$$p_* = \frac{\tilde{c}_R p_L + \tilde{c}_L p_R}{\tilde{c}_L + \tilde{c}_R} - \frac{\rho_1\left(\tilde{c}_L{}^2 + \tilde{c}_R{}^2\right)}{4\left(\tilde{c}_L + \tilde{c}_R\right)}(V_R - V_L) \tag{16}$$

Thus, the dissipation is scaled to the convective speed, which is an appropriate scale for low Mach number flows. Those were derived from the time derivative pre-conditioning method, but *a simpler and more flexible method* can be established if only the numerical dissipation in the flux is to be modified, as in SLAU [6].

The time derivative pre-conditioning is a well-established idea, and has been widely used for convergence acceleration at low speeds. However, this may not be a good option for a universally useful scheme (for low and high speed flows, and acoustic problems). For example, it requires problem-dependent adjustment for the parameter ε for a stable computation and the value is sometimes close to unity, i.e., the scheme will be reduced to the non-pre-conditioned one. The methods such as [12][13] used the ε, a byproduct of the pre-conditioning, but actually the low-speed scaling is not restricted to that particular manner. Therefore, in order to construct a potentially more practical scheme, we will borrow a different idea that has been used to construct the parameter-free all-speed AUSM family scheme [6], in contrast with the conventional, pre-conditioning-based methods. The key is the numerical speeds of sound controlled by a smooth function of a multidimensional (absolute) Mach number. Here we consider the following form for the numerical speeds of sound;

$$\tilde{c}_{L/R} = f(\bar{M}_{L/R})c_{L/R} \tag{17a}$$

$$\bar{M}_{L/R} = \sqrt{u_{L/R}{}^2 + v_{L/R}{}^2 + w_{L/R}{}^2}\,/\,c_{L/R} \tag{17b}$$

The following behaviors are required for the non-dimensional function f in order to control the scale of the embedded numerical dissipation;

$$f\begin{cases}\propto \hat{M}_{L/R} & \hat{M}_{L/R} << 1 \\ = 1 & \hat{M}_{L/R} \geq 1\end{cases} \tag{18}$$

Furthermore, its positivity is required in order to prevent anomalous behaviors at the stagnation. One of the simplest definitions for the smooth function can be given by;

$$f_{L/R} = \hat{M}_{L/R}\left(2 - \hat{M}_{L/R}\right) \tag{19a}$$

$$\hat{M}_{L/R} = \min\left(1, k\sqrt{{M_{L/R}}^2 + {M_c}^2}\right) \tag{19b}$$

The form of Eq. (19a) was initially proposed in [5]. Here M_c, "cutoff Mach number," is a positive non-dimensional parameter introduced to prevent anomalous behaviors at the stagnation and having the scale of uniform Mach number. Moreover, $k \approx O(1)$ is a positive, arbitrary, non-dimensional parameter of the order of unity [30]. Note that Eq.(19b) is slightly different from a conventional form of $\hat{M}^2_{L/R} = \min\left(1, k\max\left({M_{L/R}}^2, {M_c}^2\right)\right)$ such as in [13]. As demonstrated in Fig. 2, the present form (${M_{L/R}}^2 + {M_c}^2$, denoted as "sum") attains more smooth transition than the conventional one ($\max\left({M_{L/R}}^2, {M_c}^2\right)$, "max") around the cutoff Mach number M_c.

Let us turn our attention to the mass flux. It has been known that the pressure difference term in the mass flux function has significant influences on the solution quality [5, 6, 8, 16]. Thus, the following form will be used for the signal speed to control this term.

$$s_* = \frac{\alpha_L V_L + \alpha_R V_R}{\alpha_L + \alpha_R} - \theta\frac{\Delta p}{\alpha_L + \alpha_R} = \frac{\alpha_L V_L + \alpha_R V_R}{\alpha_L + \alpha_R} - \theta\frac{\Delta p}{\rho_L \tilde{c}_L + \rho_R \tilde{c}_R} \tag{20}$$

When θ is unity, the original form of Batten et al. [15] is recovered.

It can be seen that the amount of the pressure dependent term will be magnified if the numerical speed of sound is reduced. Note that the scaling of the pressure term also by the numerical speed of sound is favorable to suppress wiggles for very low Mach number flows [16]. However, according to our preliminary survey, it lowers the allowable Courant number (in consistent with [33, 34]), and more importantly, damps sound propagations excessively. Thus, the following definition of θ is introduced to scale the pressure difference only when necessary, for both the aerodynamic and aero-acoustic simulations.

$$\theta = \frac{\alpha_L + \alpha_R}{\alpha_{L0} + \alpha_{R0}} \tag{21a}$$

$$\alpha_{L0} = \rho_L (V_L - s_{L0}), \quad \alpha_{R0} = \rho_R (s_{R0} - V_R) \tag{21b}$$

$$s_{L0} = \min(V_L - c_L, V_R - c_R), \quad s_{R0} = \max(V_R + c_R, V_L + c_L) \tag{21c}$$

Note that $\theta \approx O(M)$ at low speeds, since the numerator in Eq.(21a) is $O(\rho c M)$ while the denominator is $O(\rho c)$. At high speeds ($\theta \geq 1$, since both the numerator and the denominator in Eq.(21a) are $O(\rho c)$), on the other hand, and the dependency of s_* on pressure goes back to that of the original form expressed by Eq.(9). This scheme is denoted as HLLCL (HLLC with Low-dissipation), and its complete form is summarized in Appendix A, and its dissipation is analyzed in Appendix B. The original HLLC formulation is recovered if Mach number is high ($M > 1$).

3. Numerical Examples

In order to investigate the validity of the new scheme, a set of selected, simple 1D and 2D cases will be computed by HLLC, HLLCL and HLLCL (θ=1) [in which θ is taken to be unity in Eq.(15), corresponding to s_* by Batten et al. [15]], and their results will be compared. For HLLCL and HLLCL (θ=1), k=2, which is within the common choice [30], is adopted unless noted otherwise. It is common practice to set the cutoff Mach number, M_c, as the order of the freestream Mach number. However, M_c is intentionally set small in 3.4. and 3.5. where small velocity regions exist. In 3.2, in which no freestream exists, M_c is set as 10 times the initial velocity. Again, it is not our intention to illustrate better performances of HLLCL or HLLCL (θ=1) than HLLC or SLAU in every case. Instead, it will be demonstrated that our new flux functions, developed based on our AUSM-like expression of HLLC, can handle low, mild, and high speed flows and also acoustic problems with reasonable solutions.

3.1 Standard 1D shock tube

In the Sod's standard shock tube problem, the left and right side values are given as the following.

$$\begin{aligned} (\rho_L, u_L, p_L) &= (1 \quad 0 \quad 1) \\ (\rho_R, u_R, p_R) &= (0.1 \quad 0 \quad 0.125) \end{aligned} \tag{22}$$

The cutoff Mach number for HLLCL and HLLCL (θ=1) is set to be 0.05, that means these schemes are tuned for low Mach number flows (i.e., the acoustic speed will be nearly scaled to a larger value of the local velocity and Mach 0.05). A first order spatial difference and Euler explicit time integration are used. Courant number used for

HLLC, and HLLCL is 0.95 while that for HLLCL (θ=1) is 0.16 which is close to the stability limit according our preliminary numerical experiments. This limitation, in consistent with [33, 34], is due to large numerical dissipation in the mass flux term of HLLCL (θ=1) while it is suppressed in HLLCL by the function θ defined in Eq.(21a). It is seen in Fig. 3 that HLLC and HLLCL give close results to each other, except for a tiny overshoot at the expansion in HLLCL (probably due to insufficient dissipation); however, the solution of HLLCL (θ=1) is further smeared at the expansion wave front ($x \approx 0.3$), and also at the shock ($x \approx 0.9$). This is also the consequence of enhancement of the numerical dissipation in the mass flux term. Nevertheless, these solutions do not differ significantly, demonstrating the potential of the present AUSM-like expression of HLLC.

3.2 One-dimensional sound propagation

One-dimensional sound propagating towards the positive direction by setting the sinusoidal wave condition at x=0 is simulated. The computational conditions are given bellow

- Spatial discretization: Third-order MUSCL without slope limiter
- Time integration: Second order, two-step explicit scheme
- Courant number: 0.01
- Specific heat ratio: γ=1.4
- Total number of grid points per wavelength (ppw) : 40
- Number of time steps: 25000
- (Initial) Velocity amplitude: $1\text{x}10^{-3}$
- Cutoff Mach number: 0.01 (10 times the initial velocity, meaning that the dissipation associated with acoustic speed is scaled down to Mach 0.01)

Here 40ppw is the nearly the least number of grids to compute sound propagation without visible decay. Velocity profiles are shown in Fig. 4. It is seen that the wave propagates without decay by HLLC and HLLCL; on the other hand, their significant damping is observed in HLLCL (θ=1). This is again the consequence of enhancement of numerical dissipation in the last term of the mass flux term. Thus, a proper control of the dissipation such as in HLLCL is found effective for acoustic problems.

3.3 Steady flows around NACA0012 Airfoil

Inviscid and transonic (M=0.7), subsonic (M=0.1) and low Mach number (M=0.01 and 0.001) flows around NACA0012 airfoil are computed using the three schemes, and the pressure distributions on the surface are compared in Figs. 5, 6 for M=0.7, 0.1, and 0.01. The angle of incidence is three degrees and the second-order MUSCL reconstruction is used. The van Albada's slope limiter [17] is applied for transonic flows. TC-PGS1 implicit method [18] is utilized for time integration. As for control parameters for the scheme, the cutoff Mach number is set to be the freestream Mach number, and k=2 is used. Only little difference is found between the results of HLLC, HLLCL, and HLLCL (θ=1), at each Mach number except for HLLC at M=0.01 where the pressure peak at the leading edge shows disagreement with others due to too much numerical dissipation of HLLC (Fig. 6). Also, we can observe small wiggles at the trailing edge ($x \approx 1$) in the solution of HLLCL (Fig. 6).

In addition, for a very low Mach number case, the pressure distributions at M=0.001 by three schemes are shown in Fig.7. The result by HLLC shows an unphysical solution due to huge numerical dissipation and that of HLLCL shows violent oscillations near the trailing edge ($x \approx 1$) due to lack of enough dissipation. Moreover, M_c had to be set to be twice of freestream Mach number only in this very low Mach number HLLCL case in order to stabilize the computation.

Contours of the pressure coefficients at M=0.001 around the airfoil by HLLCL, HLLCL (θ=1) and HLLC are shown in Figs. 8,9 and 10. Wiggles due to lack of enough numerical dissipation around the tailing edge are found in the solution of HLLCL (Fig. 8), and an unphysical solution by HLLC is evident in Fig.10, while a physically correct solution is obtained by HLLCL (θ=1) (Fig. 9).

Recall that HLLCL (θ=1) has too much dissipation for sound propagation as opposed to the others. Therefore, it can be said that an ability to compute sound propagation and very low Mach number flows at the same time has been indeed improved by HLLCL, but not perfectly. Note that no special consideration for CFL limit is needed thanks to the implicit method employed [18] in these cases.

Then, additional subsonic cases are computed for several Mach numbers at zero angle of incidence, and the drag coefficients are compared (Fig. 11). Theoretically, the aerodynamic drag should be zero for a subsonic, inviscid flow around a two-dimensional object, and hence, this drag indicates the overall error due to the numerical dissipation. While the new HLLCL and HLLCL (θ=1) schemes exhibit only small change with respect to the Mach number, the drag for the original HLLC exhibit rapid increase as the Mach number diminishes. (Note that the drag coefficients are shown in log scale.) This is due to excessive numerical dissipation contained in the interface pressure mentioned

in 2.3. [The difference between HLLCL and HLLCL (θ=1) seems to be resulting from the treatment of θ (as explained in Appendix B), which may be improved further for error reduction. Such a work, however, is beyond the scope of the present paper.]

3.4 Supersonic Flow over Cylinder

This numerical test has been conducted by many researchers, after Jiang and Shu computed it as a benchmark test in [20]. The freestream condition is Mach 3, and the computational grid for $i \in [0, i_{\max}]$ and $j \in [0, j_{\max}]$ is generated by the following simple formula so that one of the grid lines fits the captured shockwave.

$$x_{i,j} = \left(R_x - \left(R_x - 1\right) i / i_{\max}\right) \cos\left(\theta\left(2\, j / j_{\max} - 1\right)\right) \tag{23a}$$

$$y_{i,j} = \left(R_y - \left(R_y - 1\right) i / i_{\max}\right) \sin\left(\theta\left(2\, j / j_{\max} - 1\right)\right) \tag{23b}$$

where R_x =3, R_y = 6, θ = 5π/12, $i_{\max}$ = 80 (circumferential direction), and $j_{\max}$ = 60 (wall-normal direction). The computational grid is displayed in Fig. 12a, in which the inflow condition is applied at the left boundary, the slip condition at the wall, and the top and the bottom are the outflow. The computations are carried out with MUSCL (κ=1/3) with minmod limiter for spatial reconstruction, and the two-stage, second-order, standard Runge-Kutta method for time integration. The Courant number is 0.5, and the computations converged around 20,000 timesteps.

Figures 12b and 12c show the solutions (pressure contours) by HLLCL and HLLCL (θ=1), respectively (k=1, M_c =0.1 for both, where the low speed scaling is activated only around the stagnation point). Those solutions are free from carbuncle or other shock anomalies.

3.5 Laminar Boundary-Layer over Flat Plate

A Mach 0.2 flow over a flat plate is solved in order to investigate boundary-layer resolutions. This problem has been conducted by the authors to assess the performance of a numerical scheme in viscous flows [21, 22]. The rectangular computational domain comprises 60 (streamwise) x 40 (wall-normal) cells clustered to the bottom wall and the leading-edge. The first 10 cells are in a buffer region (symmetry condition at the bottom), and the flat plate (no-slip boundary condition at the bottom) starts from the 11th cell in the stream direction. The left boundary is the inflow, and the right and the top are the outflow with the freestream pressure specified. The MUSCL (κ=1/3) is employed for special reconstruction without a slope limiter, the second-order central difference is applied to

compute the viscous flux, and the two-stage, second-order, standard Runge-Kutta method is used for time integration.

The present computations using HLLCL and HLLCL (θ=1) were carried out (k=1, M_c =0.1) for 50,000 time steps (at which the density residuals dropped three orders) with Courant number being 0.5. As seen in Fig. 13, those solutions (velocity profiles along i = 30; x= 0.4852E-02 from the leading-edge) agree well with the Blasius solution as HLLC, in contrast with the very diffusive HLLE [23]. Therefore, the new fluxes can be used in viscous flows.

As seen, HLLCL attained nearly the same solution as HLLC in the shocktube problem in 3.1; it can compute sound waves without severe decay in 3.2; it is applicable to low Mach numbers at which HLLC showed huge numerical errors (3.3). Other examples in 3.4 and 3.5 showed typical solutions obtained by HLLCL for a supersonic flow over a blunt-body and a subsonic flow over a flat plate (laminar boundary-layer). Its extension to supercritical fluids governed by a more general equation-of-state is currently ongoing [19], as briefly introduced in Appendix C. Further examinations on HLLCL will follow in Appendices D, E, and F.

4. Conclusions

The HLLC numerical flux function has been expressed in AUSM-like formulation. Then, the simple idea already incorporated in AUSM family schemes (as opposed to the time-derivative preconditioning) is applied to HLLC scheme for all-speed simulations, i.e., HLLCL (HLLC with Low-dissipation) has been developed. In the course of its derivation, the embedded numerical dissipation of HLLC scheme has been analyzed, and the signal speeds in HLLC scheme has been modified so as to have appropriate scales at low speeds. Numerical experiments demonstrated that the HLLCL can compute flows of a wide range of Mach numbers accurately as well as sound propagations.

This facilitates its extensions to fluids governed by general equations-of-state, such as multiphase flows and supercritical fluids. Such a topic is ongoing as a separate work. An extension to multidimensional, unstructured grids is straightforward and also left as a future work.

Acknowledgements

The authors appreciate Dr. Nonomura at ISAS/JAXA (currently at Tohoku University) for having valuable discussions with us.

Appendix A: HLLCL Formulation

The formulation of HLLCL is summarized here.

$$\widetilde{E}_{HLLCL} = \frac{\dot{m}+|\dot{m}|}{2}\mathbf{\Phi'}_L + \frac{\dot{m}-|\dot{m}|}{2}\mathbf{\Phi'}_R + \widetilde{p}\mathbf{N} \tag{A.1a}$$

$$\mathbf{\Phi'}_{L/R} = \mathbf{\Phi}_{L/R} + \begin{pmatrix} 0 & 0 & 0 & 0 & \dfrac{\widetilde{s}_{L/R}\left(p_* - p_{L/R}\right)}{\rho_{L/R}\left(s_{L/R} - V_{L/R}\right)} \end{pmatrix}^T \tag{A.1b}$$

$$\mathbf{\Phi} = \left(1, u, v, w, h\right)^T \tag{A.1c}$$

$$\mathbf{N} = \left(0, x_n, y_n, z_n, 0\right)^T \tag{A.1d}$$

$$h = (e + p)/\rho \tag{A.1e}$$

where the mass flux and the pressure flux are given as

$$\dot{m} = \begin{cases} \rho_L V_L + \widetilde{s}_L\left(\rho_{L*} - \rho_L\right) & s_* > 0 \\ \rho_R V_R + \widetilde{s}_R\left(\rho_{R*} - \rho_R\right) & otherwise \end{cases} \tag{A.2a}$$

$$\widetilde{p} = p_* + \begin{cases} \dfrac{s_*}{s_* - \widetilde{s}_L}\left(p_L - p_*\right) & s_* > 0 \\ \dfrac{s_*}{s_* - \widetilde{s}_R}\left(p_R - p_*\right) & otherwise \end{cases} \tag{A.2b}$$

with

$$\rho_{L/R*} = \frac{s_{L/R} - V_{L/R}}{s_{L/R} - s_*}\rho_{L/R} \tag{A.2c}$$

$$\widetilde{s}_L = \min(0, s_L), \quad \widetilde{s}_R = \max(0, s_R) \tag{A.2d}$$

$$\alpha_L = \rho_L\left(V_L - s_L\right) > 0, \quad \alpha_R = \rho_R\left(s_R - V_R\right) > 0 \tag{A.2e}$$

$$V = x_n u + y_n v + z_n w \tag{A.2f}$$

$$p_* = \frac{1}{2}\{p_L + p_R + \alpha_L(V_L - s_*) - \alpha_R(V_R - s_*)\} \tag{A.2g}$$

The left and right signal speeds are

$$s_L = \min(V_L - \tilde{c}_L, V_R - \tilde{c}_R), \quad s_R = \max(V_R + \tilde{c}_R, V_L + \tilde{c}_L) \tag{A.3a}$$

$$\tilde{c}_{L/R} = c_{L/R}\hat{M}_{L/R}\left(2 - \hat{M}_{L/R}\right) \tag{A.3b}$$

$$\hat{M}_{L/R} = \min\left(1, k\sqrt{{M_{L/R}}^2 + {M_c}^2}\right) \tag{A.3c}$$

$$M_{L/R} = \sqrt{{u_{L/R}}^2 + {v_{L/R}}^2 + {w_{L/R}}^2}\,/\,c_{L/R} \tag{A.3d}$$

where M_c is the cutoff Mach number having the scale of uniform Mach number, and $k \approx O(1)$ is a positive non-dimensional parameter of the order of unity. Finally, the convective signal speed is given as follows.

$$s_* = \frac{\alpha_L V_L + \alpha_R V_R}{\alpha_L + \alpha_R} - \theta\frac{\Delta p}{\alpha_L + \alpha_R} \tag{A.4}$$

where

$$\theta = \frac{\alpha_L + \alpha_R}{\alpha_{L0} + \alpha_{R0}} \tag{A.5a}$$

$$\alpha_{L0} = \rho_L\left(V_L - s_{L0}\right), \quad \alpha_{R0} = \rho_R\left(s_{R0} - V_R\right) \tag{A.5b}$$

$$s_{L0} = \min(V_L - c_L, V_R - c_R), \quad s_{R0} = \max(V_R + c_R, V_L + c_L) \tag{A.5c}$$

Appendix B: Dissipation of HLLCL

As in [35], the dissipation term in the pressure flux is analyzed for low speeds. Now let $s_* > 0$ and $|M_L| << 1$, $|M_R| << 1$,

$$\begin{aligned}\theta &= \frac{\alpha_L + \alpha_R}{\alpha_{L0} + \alpha_{R0}} \\ &\to \frac{2\rho_L c_L[M_c] + 2\rho_R c_R[M_c]}{\rho_L c_L + \rho_R c_R} \\ &\to \frac{4\overline{\rho c}[M_c]}{2\overline{\rho c}} = 2[M_c]\end{aligned} \tag{B.1}$$

where $[x]$ denotes "the order of x."

$$
\begin{aligned}
s_* &= \frac{\alpha_L V_L + \alpha_R V_R}{\alpha_L + \alpha_R} - \theta \frac{\Delta p}{\alpha_L + \alpha_R} \\
&\to \frac{2\rho_L c_L V_L [M_c] + 2\rho_R c_R V_R [M_c]}{2\rho_L c_L [M_c] + 2\rho_R c_R [M_c]} - \theta \frac{\Delta p}{2\rho_L c_L [M_c] + 2\rho_R c_R [M_c]} \\
&\to \frac{4\overline{\rho c}^2 [M_c][M]}{4\overline{\rho c}[M_c]} - \theta \frac{\overline{\rho c}^2 [M^2]}{4\overline{\rho c}[M_c]} \\
&\to \begin{cases} \bar{c}[M] - \dfrac{\bar{c}[M^2]}{2}, & (\theta \to 2[M_c]) \\ \bar{c}[M] - \dfrac{\bar{c}[M^2]}{4[M_c]}, & (\theta = 1) \end{cases}
\end{aligned}
\tag{B.2}
$$

Then, after some manipulation for $[M] = [M_c]$, the pressure flux leads to

$$
\begin{aligned}
\tilde{p} &= p_* + \frac{s_*}{s_* - \tilde{s}_L}(p_L - p_*) \\
&= \frac{1}{2}(p_L + p_R) + \frac{\alpha_L (V_L - s_*) - \alpha_R (V_R - s_*)}{2} + \frac{s_*}{s_* - \tilde{s}_L}(p_L - p_*) \\
&= \frac{1}{2}(p_L + p_R) + \cancel{(\rho_L c_L^2 - \rho_R c_R^2)[M^2]} - \cancel{(\rho_L c_L - \rho_R c_R)[M] s_*} \\
&+ \frac{s_*}{s_* - \tilde{s}_L}\left(-\frac{\Delta p}{2} - \cancel{\frac{\alpha_L V_L - \alpha_R V_R}{2}} - \cancel{\frac{\alpha_R - \alpha_L}{2} s_*} \right) \\
&\to \begin{cases} \dfrac{1}{2}(p_L + p_R) - \dfrac{1}{4}\overline{\rho c}^2 [M^2], & (\theta \to 2[M_c]) \quad \boxed{\text{HLLCL}} \\ \dfrac{1}{2}(p_L + p_R) - \dfrac{3}{14}\overline{\rho c}^2 [M^2], & (\theta = 1) \quad \boxed{\text{HLLCL } (\theta=1)} \end{cases}
\end{aligned}
\tag{B.3}
$$

Central Difference Dissipation

by assuming $\rho_L = \rho_R = \overline{\rho}$ and $c_L = c_R = \overline{c}$. As seen from this rough approximation, HLLCL and HLLCL (θ=1) have similar but slightly different dissipation at low speeds if $[M] = [M_c]$. (This supports slightly different numerical errors by HLLCL and HLLCL (θ=1) in Fig. 11.)

Appendix C: Extension to Supercritical Fluids

In a separate work [19], AUSM family schemes have been extended to supercritical fluids expressed by a complicated, cubic, Soave-Redlich-Kwon (SRK) EOS [24], expressed as follows:

$$p = \frac{RT}{V-b} - \frac{a(T)}{V^2 + bV} \tag{C.1}$$

$$a(T) = \frac{0.042747 R^2 T_{cr}^2}{p_{cr}} \cdot \left\{ 1 + f_\omega \cdot \left(1 - \sqrt{\frac{T}{T_{cr}}} \right)^2 \right\} \tag{C.2}$$

$$b = \frac{0.08664 R T_{cr}}{p_{cr}} \tag{C.3}$$

$$f_\omega = 0.48 + 1.574\omega - 0.176\omega^2 \tag{C.4}$$

where T_{cr} and p_{cr} are critical temperature (126.2 K for nitrogen) and critical pressure (3.4 MPa for nitrogen), respectively, and ω is acentric factor (ω=0.0372 for nitrogen). The (universal) gas constant R = 8.3144 J/(mol K), and the specific volume V is $V = M/\rho$, where M is molecular weight (M = 0.028 kg/mol for nitrogen), and ρ is density.

The "AUSM family" mentioned above does not exclude HLLCL, of course, and the corresponding formulation solves the following pressure-equilibrium equation [25] (for the Euler equation, for brevity), instead of the energy equation.

$$\frac{p^{n+1}{}_i - p^n{}_i}{\Delta t} + \frac{1}{\Omega_i} \left[\sum_j (pV_n)_{i,j} S_{i,j} + (\rho_i c_i^2 - p_i) \sum_j (V_n)_{i,j} S_{i,j} \right] = 0 \tag{C.5a}$$

$$V_n = \frac{\dot{m} + |\dot{m}|}{2} \frac{1}{\rho_L} + \frac{\dot{m} - |\dot{m}|}{2} \frac{1}{\rho_R} \tag{C.5b}$$

$$pV_n = \frac{\dot{m} + |\dot{m}|}{2} \frac{p_L}{\rho_L} + \frac{\dot{m} - |\dot{m}|}{2} \frac{p_R}{\rho_R} \tag{C.5c}$$

where c_i is the speed of sound at cell i, and V_n is the velocity (outward) normal to the cell-interface [please notice its similarity with Eq.(2)]. This treatment suppresses numerical oscillations appearing around the abrupt changes of variables.

A moving nitrogen contact discontinuity [26], initially located at x=0.3m, represents the numerical solutions. 100 cells are evenly spaced for a [0, 1] m domain (i.e., the grid spacing Δx=0.01m), and the initial conditions are given as follows.

$(\rho, u, p, T)_L$ = (450.0kg/m^3, 10.0m/s, 4.0MPa, 124.6K) for $x \leq$0.3m

$(\rho, u, p, T)_R$ = (45.0kg/m^3, 10.0m/s, 4.0MPa, 298.5K) for x>0.3m

where the left boundary condition is the inflow, and the right boundary is the outflow with the prescribed pressure. The computations are conducted with Δt=1.0×10^{-5}s (Courant number ≈ 0.4), up to 0.04s (4,000 steps). The solutions are displayed in Fig. C.1 [19], demonstrating that the extended HLLCL [by Eq. (C.5)] preserves constancy of pressure while the original one fails. Please see [19] for other examples.

Appendix D: Effects of Two Parameters (k, M_c)

Now let us briefly check the influences of the selections of the two parameters (k, M_c) included in HLLCL. Selected results are shown in Fig. D.1 for 3.4 Supersonic Flow over Cylinder, and Fig. D.2 for 3.5 Laminar Boundary-Layer over Flat Plate. We tested (k, M_c) = (1, 0.1) (default), (1, 1.0), (0.1, 0.1), and (2, 0.1). As seen from those figures, the solutions look insensitive to the chosen values of (k, M_c) as long as they are big enough, whereas (k, M_c) = (0.1, 0.1) cases diverged in both examples. In other words, the effects of these two parameters are consistent between the two numerical tests, in spite of differences in freestream Mach number and viscous effects.

Appendix E: Positivity of HLLCL

The positivity of HLLCL is assessed in the vacuum flow problem [36]. In this test, 300 uniform cells are used separated at the very center by the left condition, i.e., $(\rho, u, e)_L^T$ = (1, -2, 3), and the right condition, i.e., $(\rho, u, e)_R^T$ = (1, 2, 3). The left and right boundaries are the outflow. The MUSCL (κ=1/3) is employed for special reconstruction with Van Albada's slope limiter (ε=1.e-6), and the two-stage, second-order, standard Runge-Kutta method is used for time integration.

The present computations using HLLCL and HLLCL (θ=1) were carried out (k=1, M_c =0.1) for 100 time steps with Δt = 0.2 (the corresponding Courant number is about 0.54). It is confirmed that they successfully conserved the positivity, reaching almost the same results (Fig. E.1), whereas Roe flux failed to obtain the solutions.

Appendix F: Severe Hypersonic Problem

It is reported that many numerical fluxes fail to produce a stable and symmetry bow shock ahead of a cylinder at hypersonic speeds, particularly when computational cells have a large aspect ratio [37, 38, 39]. We have conducted such Mach 20 cases [37] with 800 cells in the circumferential direction and 30 cells in the wall-normal direction, covering a fan-shaped space of ±75 degrees upstream the cylinder. First-order accurate methods are employed both in space and time (i.e., Euler explicit method), and the computations are run with CFL=0.5 for 40,000 steps.

The solutions are showin in Fig. F.1. HLLCL exhibit the carbuncle-like solution, and HLLCL (θ=1) yielded the full carbuncle, whereas SLAU2 showed only slight asymmetry. This comes with no surprise, since the proposed methods recover to the original HLLC (which is known to be carbuncle-prone, as well as the Roe flux) at supersonic speeds. These could be remedied by a multi-dimensional dissipation strategy, e.g. in [37, 40, 41, 42], and the research in this direction is ongoing. Nevertheless, we have demonstrated that HLLC can be expressed in the AUSM form, and also that it is extendable to all speeds by the same strategy as in the AUSM-family (such as SLAU). These are our initial objectives of the present study and have been successfully acomplished.

References

[1] Van Leer, B.: Towards the Ultimate Conservative Difference Scheme. V. A Second-Order Sequel to Godunov's Method, *J. Comput. Phys.*, Vol. 32 (1979), pp.101-136.

[2] Toro, E., F., Spruce, M. and Speares, W.: Restoration of the Contact Surface in the HLL-Riemann Solver, *Shock Waves*, Vol.4, (1994), pp. 25-34.

[3] Liou, M.S. and Steffen Jr., C.J.: A New Flux Splitting Scheme, *J. Comput. Phys.*, Vol. 107(1993), pp.23–39.

[4] Liou, M.S.: A Sequel to AUSM: AUSM+, *J. Comput. Phys.*, Vol. 129 (1996), pp.364–382.

[5] Liou, M.S.: A Sequel to AUSM, Part II: AUSM+-up for All Speeds, *J. Comput. Phys.,* Vol. 214 (2006), pp. 137-170.

[6] Shima, E. and Kitamura, K.: Parameter-Free Simple Low-Dissipation AUSM-Family Scheme for All Speeds, *AIAA J.*, Vol.49, No.8 (2011), pp.1693-1709.

[7] Kitamura, K. and Shima, E.: Towards shock-stable and accurate hypersonic heating computations: A new pressure flux for AUSM-family schemes, *J. Comput. Phys.*, Vol.245 (2013), pp.62-83. doi:10.1016/j.jcp.2013.02.046

[8] Shima, E. and Kitamura, K.: Multidimensional Numerical Noise from Captured Shockwave and Its Cure, *AIAA J.*, Vol. 51, No. 4 (2013), pp.992-998. doi: 10.2514/1.J052046

[9] Shimizu, T., Hori, D., Kitamura, K., Daimon, Y., and Oyama, A.: Slit Resonator Design and Damping Estimation in

Linear and Non-linear Ranges, AIAA Paper 2011-3261, 41st AIAA Fluid Dynamics Conference and Exhibit, Honolulu, Hawaii, Jun. 2011.

[10] Van Leer, B.: Flux Vector Splitting for the Euler Equations, *Lecture Notes in Phys.*, Vol. 170 (1982), pp. 507-512.

[11] Luo, H. and Baum, J.D. and Löhner, R.: Extension of Harten-Lax-van Leer scheme for flows at all speeds, *AIAA J.,* Vol. 43, No. 6 (2005), pp.1160-1166

[12] Park, S.H., Lee, J.E., and Kwon, J.H.: Preconditioned HLLE Method for Flows at All Mach Numbers, *AIAA J.,* Vol. 44, No. 11 (2006), pp.2645-2653

[13] Weiss, J.M. and Smith, W.A.: Preconditioning Applied to Variable and Constant Density Flows, *AIAA J.*, Vol. 33, No.11 (1995), pp.2050-2057

[14] Harten, A., Lax, P. D., and van Leer, B.: On Upstream Differencing and Godunov-Type Scheme for Hyperbolic Conservation Laws, *SIAM Review*, Vol. 25, No. 1 (1983), p. 35.

[15] Batten, P., Clarke, N., Lambert, C. and Causon, D. M.: On the choice of wave speeds for the HLLC Riemann solver, *SIAM J. Sci. Stat. Comput.,* Vol. 18, No. 6, (1997), pp.1553-1570

[16] Shima, E.: On the Improvement of the All-Speed Flux Scheme for Very Low Mach Number Flows, AIAA Paper 2013-2696 (2013)

[17] Van Albada, G.D., Van Leer, B. and Roberts, Jr., W.W.: A Comparative Study of Computational Methods in Cosmic Gas Dynamics, *Astron. Astrophys.*, Vol. 108 (1982), pp.76-84.

[18] Shima, E. and Kitamura, K.: New approaches for computation of low Mach number flows, *Computers & Fluids*, Vol. 85 (2013), pp. 143–152, 10.1016/j.compfluid.2012.11.017

[19] Kitamura, K., and Shima, E.: Pressure-Equation-Based SLAU2 for Oscillation-Free, Supercritical Flow Computations, *Computers & Fluids*, Vol.163 (2018), pp.86-96. 10.1016/j.compfluid.2018.01.001

[20] Jiang, G.-S. and Shu, C.-W.: Efficient Implementation of Weighted ENO Schemes, *J. Comput. Phys.*, Vol.126 (1996), pp.202–228.

[21] Kitamura, K.: Assessment of SLAU2 and Other Flux Functions with Slope Limiters in Hypersonic Shock-Interaction Heating, *Computers & Fluids*, Volume 129 (2016), Pages 134-145

[22] Nishikawa, H. and Kitamura, K.: Very Simple, Carbuncle-Free, Boundary-Layer Resolving, Rotated-Hybrid Riemann Solvers, *J. Comput. Phys.*, Vol. 227 (2008), pp.2560-2581.

[23] Einfeldt, B.: On Godunov-Type Methods for Gas Dynamics, *SIAM Journal on Numerical Analysis*, Vol. 25 (1998), pp.294-318.

[24] Soave, G.: Equilibrium constants from a modified Redlich–Kwong equation of state, *Chemical Engineering Science*, Vol.27, No.6 (1972), pp.1197–1203.

[25] Fedkiw, R., Liu, X., and Osher, S.: A general technique for eliminating spurious oscillations in conservative schemes for multiphase and multispecies Euler equations, *International Journal of Nonlinear Sciences and Numerical Simulation*, Vol.3, No.2 (2002), pp.99–106.

[26] Terashima, H., Kawai, S., and Yamanishi, N.: High-resolution numerical method for supercritical flows with large density variations, *AIAA J.*, Vol. 49, No.12 (2011), pp.2658–2672.

[27] Chang, C.-H., Liou, M.-S.: A robust and accurate approach to computing compressible multiphase flow: Stratified flow model and AUSM+-up scheme. *J. Comput. Phys.* Vol. 225 (2007), pp. 840–873. https://doi.org/10.1016/j.jcp.2007.01.007

[28] Kitamura, K., Nonomura, T.: Simple and robust HLLC extensions of two-fluid AUSM for multiphase flow computations. *Comput.Fluids,* Vol. 100 (2014), pp. 321–335. https://doi.org/10.1016/j.compfluid.2014.05.019

[29] Liou, M.S.: Mass Flux Schemes and Connection to Shock Instability, *J. Comput. Phys.*, Vol. 160 (2000), pp. 623–648.

[30] Turkel, E.: Preconditioning Techniques in Computational Fluid Dynamics, *Annu. Rev. Fluid Mech.* Vol. 31 (1999), pp. 385–416

[31] Kim, H., Kim, H., and Kim, C.: Computations of homogeneous multiphase real fluid flows at all speeds, *AIAA Journal*, Vol. 56, No. 7 (2018), pp.2623-2634. DOI: 10.2514/1.J056497, 2018.

[32] Kim, H., Choe, Y., Kim, H., Min, D., and Kim, C.: Methods for compressible multiphase flows and their applications, *Shock Waves*, Vol. 29 (2019), pp.235-261. DOI: 10.1007/s00193-018-0829-x, 2019.

[33] Folkner, D., Katz, A., and Sankaran, V.: An unsteady preconditioning scheme based on convective-upwind split-pressure artificial dissipation, *International Journal for Numerical Methods in Fluids*, Vol. 78 (2015), pp.1-16. DOI: 10.2514/6.2014-1424.

[34] Sachdev, J., Hosangadi, A., and Sankaran, V.: Improved flux formulations for unsteady low Mach number flows, in: AIAA Paper No. 2012-3067, 42nd AIAA Fluid Dynamics Conference and Exhibit, 2012, DOI: 10.2514/6.2012-3067

[35] Kitamura, K. and Hashimoto, A.: Reduced dissipation AUSM-family fluxes: HR-SLAU2 and HR-AUSM+-up for high resolution unsteady flow simulations, *Comput.Fluids*, Vol. 126 (2016), pp.41-57.

[36] Einfeldt, B., Munz, C.D., Roe, P.L., and Sjogreen, B.: On Godunov-type methods near low density, *J. Comput. Phys.*, Vol. 92 (1991), pp.273–295.

[37] Chen, S.-S., Yan, C., Lin, B.-X., Liu, L.-Y., and Yu, J.: Affordable shock-stable item for Godunov-type schemes against carbuncle phenomenon, *J. Comput. Phys.* Vol. 373 (2018), pp.662-672. doi.org/10.1016/j.jcp.2018.07.022

[38] Kitamura, K., Shima, E., Nakamura, Y., and Roe, P.L.: Evaluation of Euler fluxes for hypersonic heating computations, *AIAA Journal*, Vol. 48, No. 4 (2010), pp.763-776. doi: 10.2514/1.41605

[39] Pandolfi, M. and D'Ambrosio, D.: Numerical Instabilities in Upwind Methods: Analysis and Cures for the "Carbuncle" Phenomenon, *J. Comput. Phys.*, Vol. 166, No. 2 (2001), pp.271-301.

[40] Kim, K.H., Kim, C., and Rho, O.H.: Methods for the Accurate Computations of Hypersonic Flows I. AUSMPW+ Scheme, *J. Comput. Phys.*, Vol. 174 (2001), pp.38-80.

[41] Sanders, R., Morano, E. and Druguetz, M.C.: Multidimensional Dissipation for Upwind Schemes: Stability and Applications to Gas Dynamics, *J. Comput. Phys.*, Vol. 145 (1998), pp.511-537.

[42] Shima, E. and Kitamura, K.: Multidimensional Numerical Noise from Captured Shockwave and Its Cure, *AIAA J.*, Vol. 51, No. 4 (2013), pp.992-998.

List of Figures

Figures

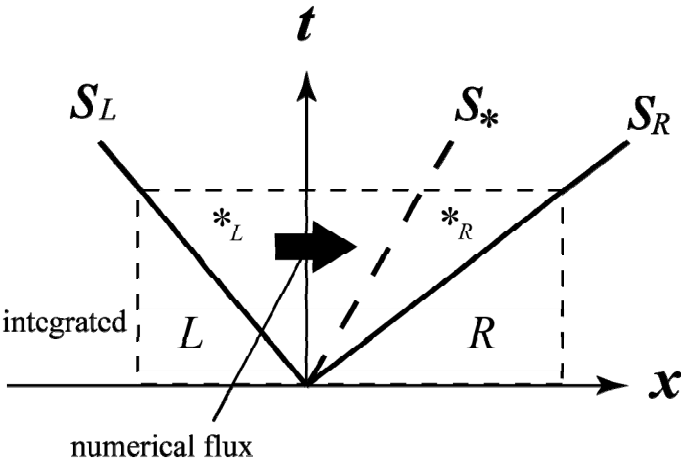

Fig. 1 Schematic of Riemann problem.

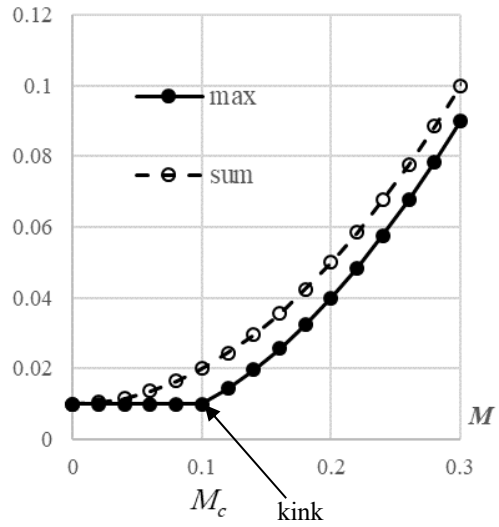

Fig. 2 Behaviors of present ("sum") and conventional ("max") Mach number expressions near the cutoff Mach number, M_c = 0.1.

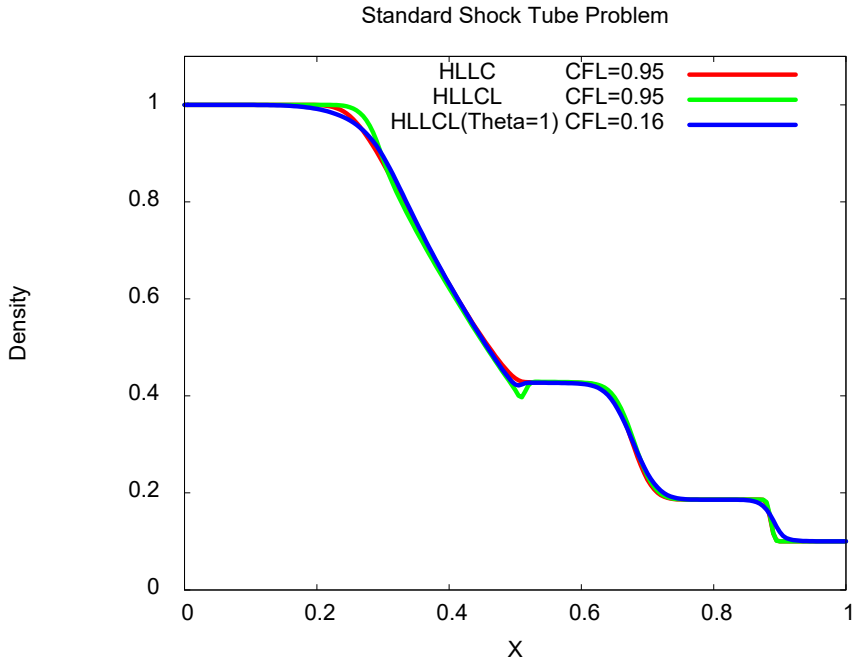

Fig. 3 Density distribution of the standard shock tube problem by HLLC, HLLCL and HLLCL (θ=1).

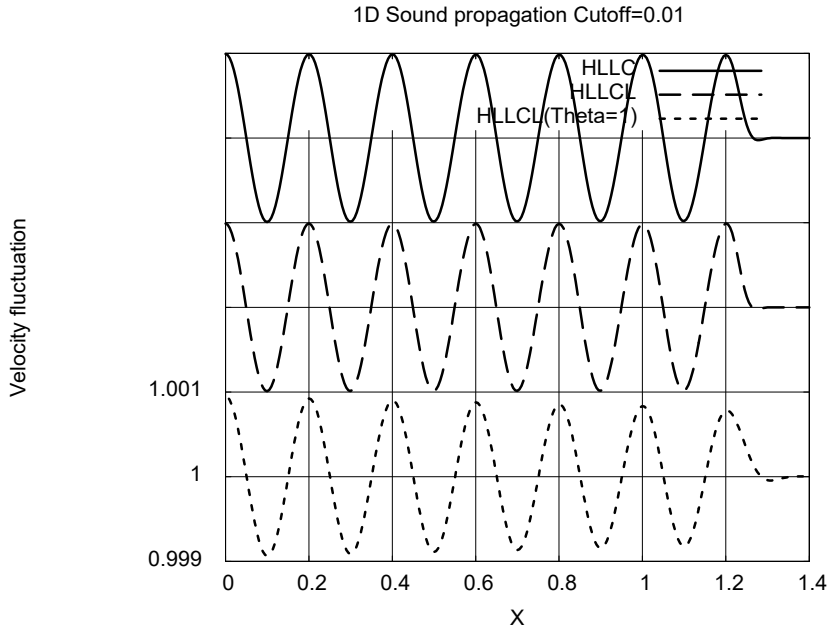

Fig. 4 Spatial velocity variations of 1-D sound propagation computed by HLLC, HLLCL and HLLCL (θ=1).

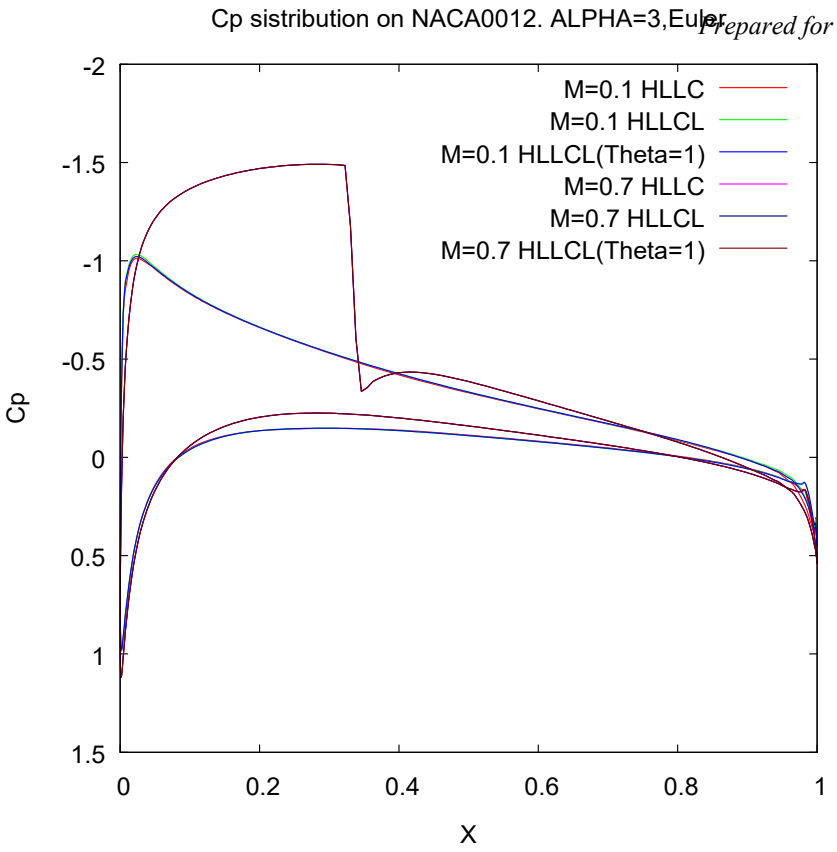

Fig. 5 Pressure distribution on NACA0012 airfoil in inviscid flows computed by three methods (M=0.1, 0.7).

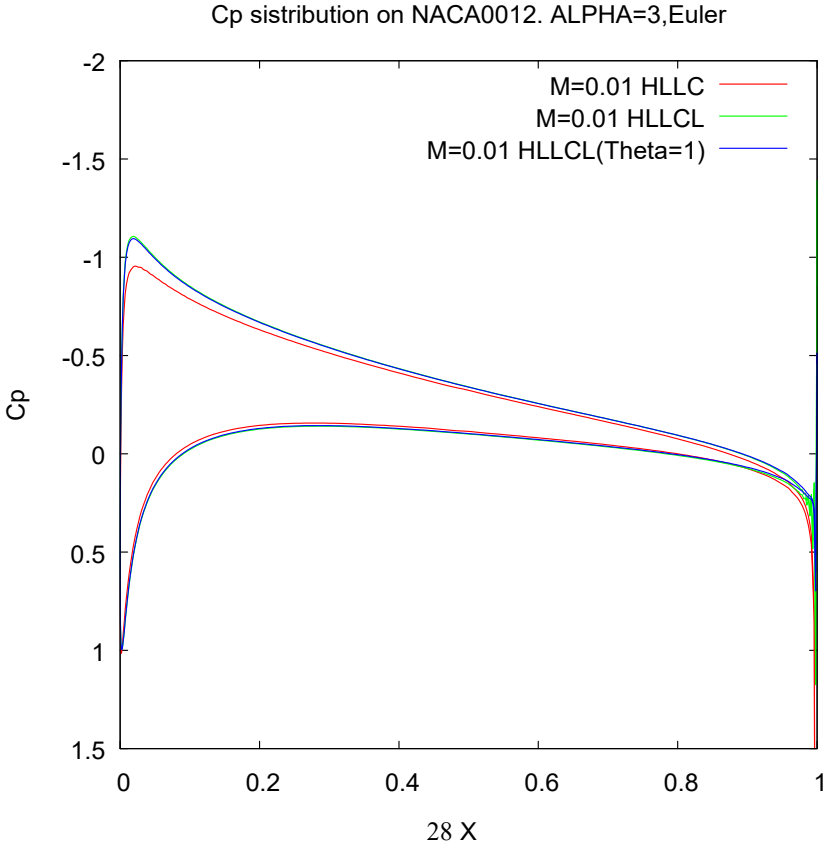

Fig. 6 Pressure distribution on NACA0012 airfoil in inviscid flows computed by three methods (M=0.01).

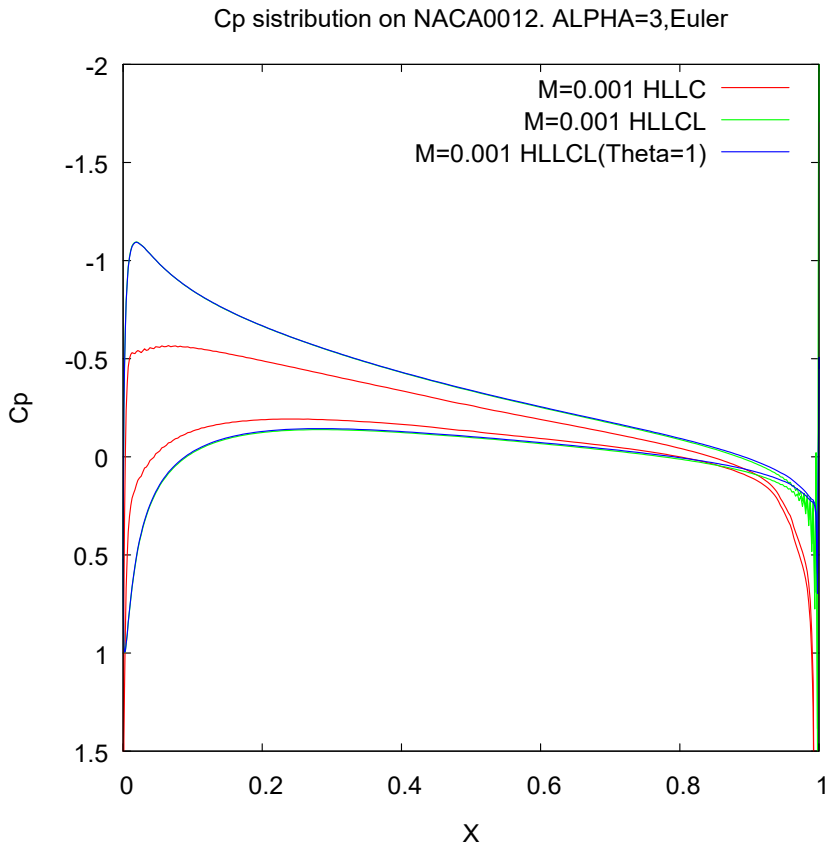

Fig. 7 Pressure distribution on NACA0012 airfoil in inviscid flows computed by three methods (M=0.001).

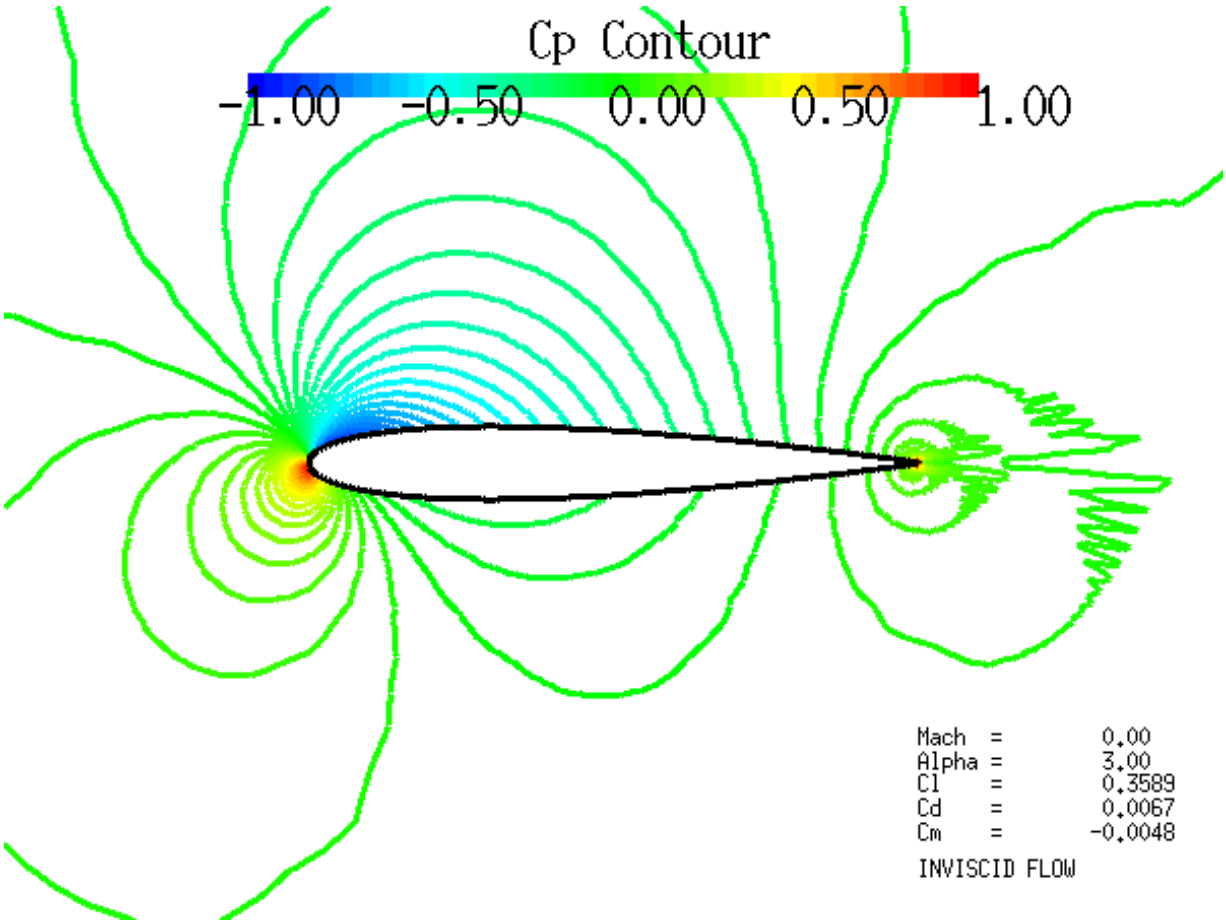

Fig. 8 Pressure contour around NACA0012 airfoil at M=0.001 by HLLCL.

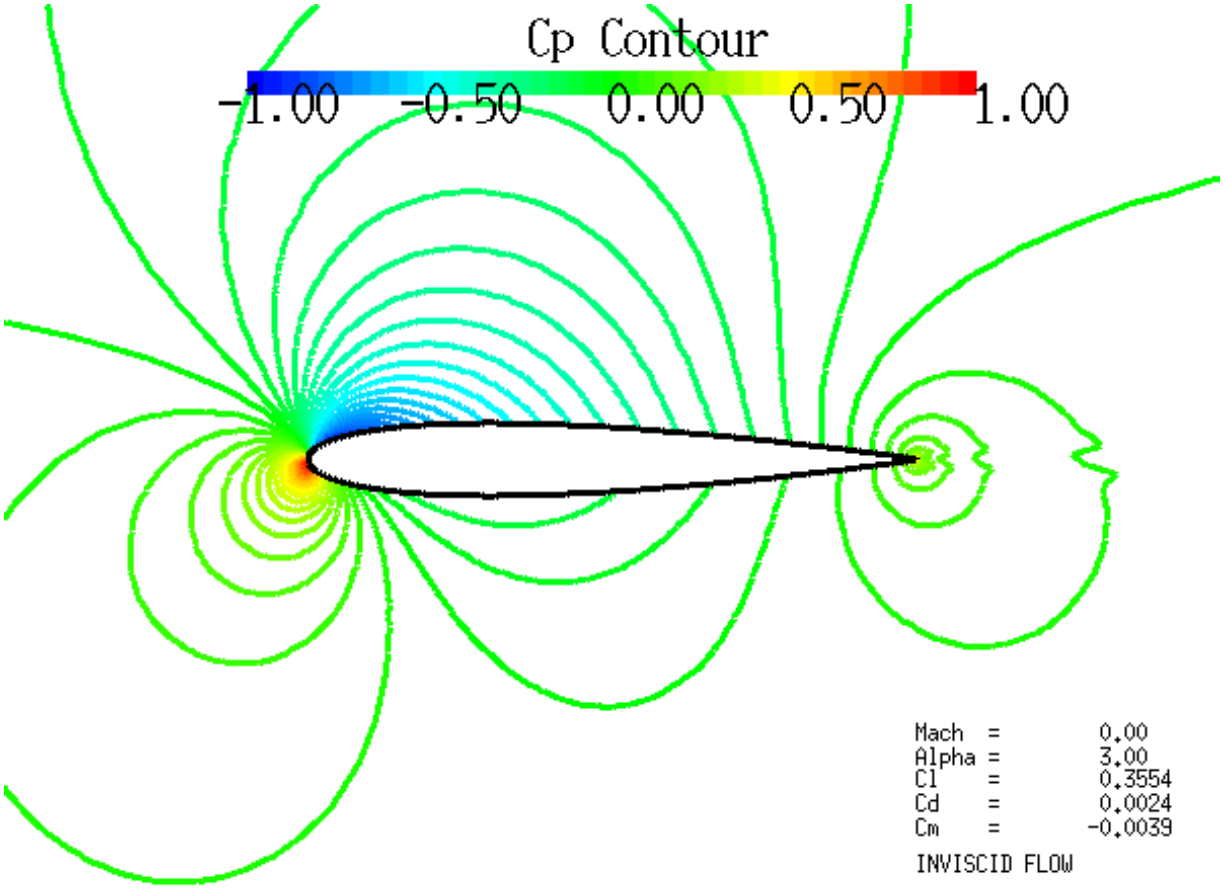

Fig. 9 Pressure contour around NACA0012 airfoil at M=0.001 by HLLCL(θ=1).

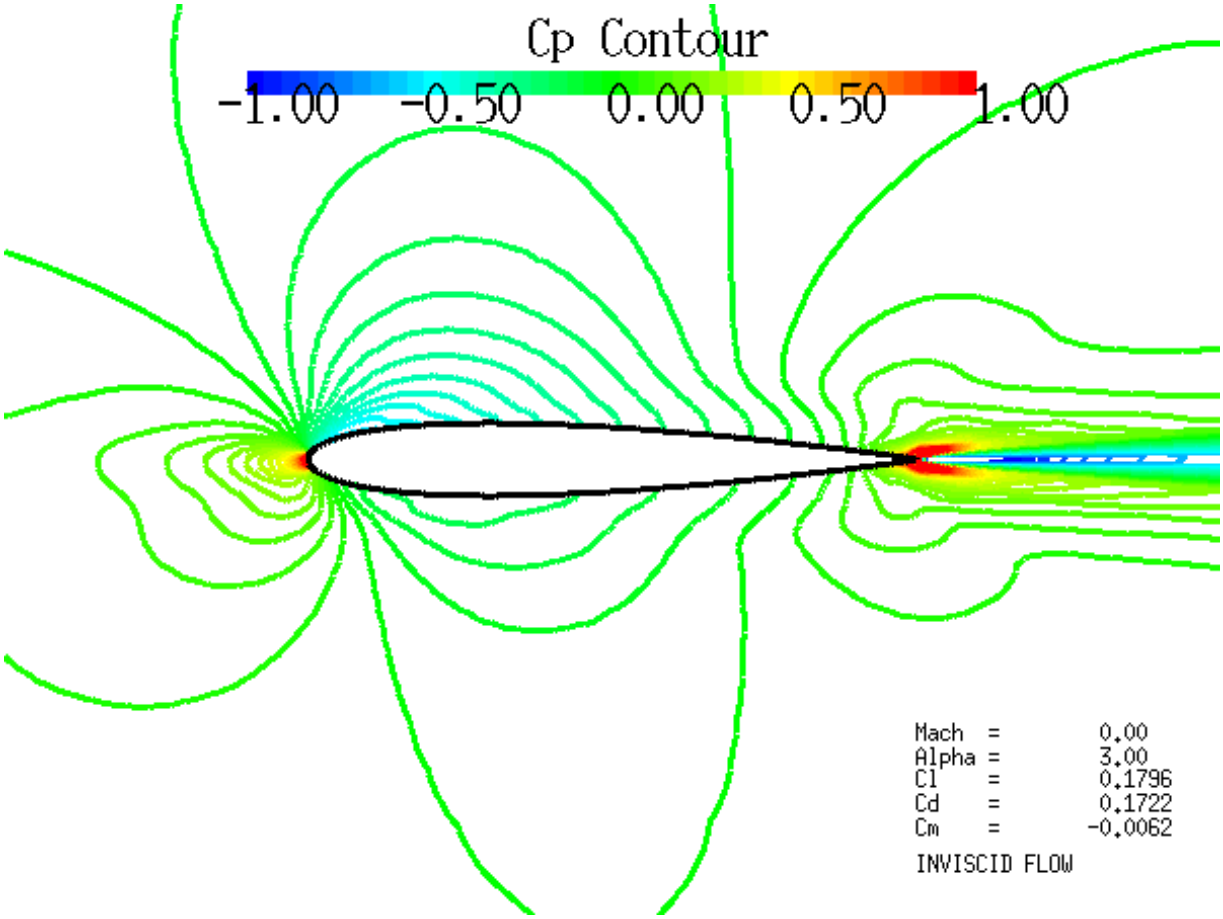

Fig. 10 Pressure contour around NACA0012 airfoil at M=0.001 by HLLC.

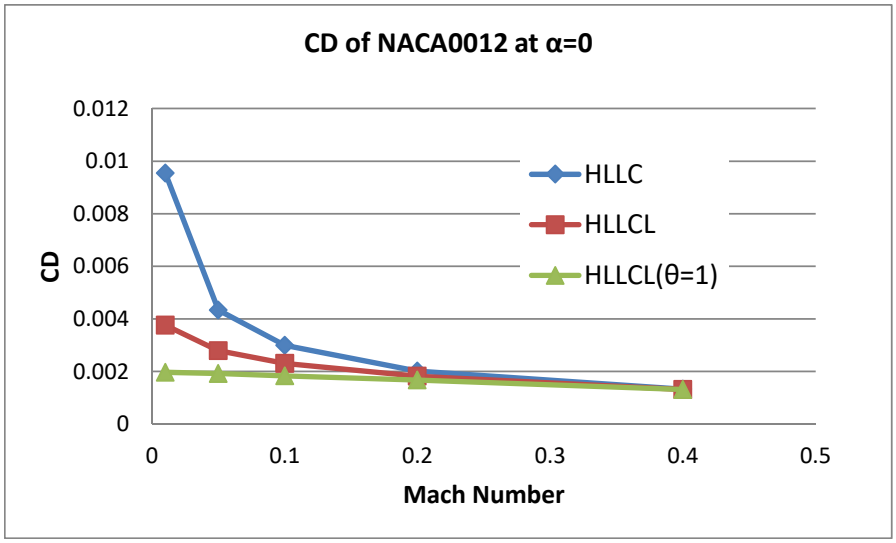

Fig. 11 Drag coefficients of NACA0012 airfoil at various Mach numbers in inviscid subsonic flows.

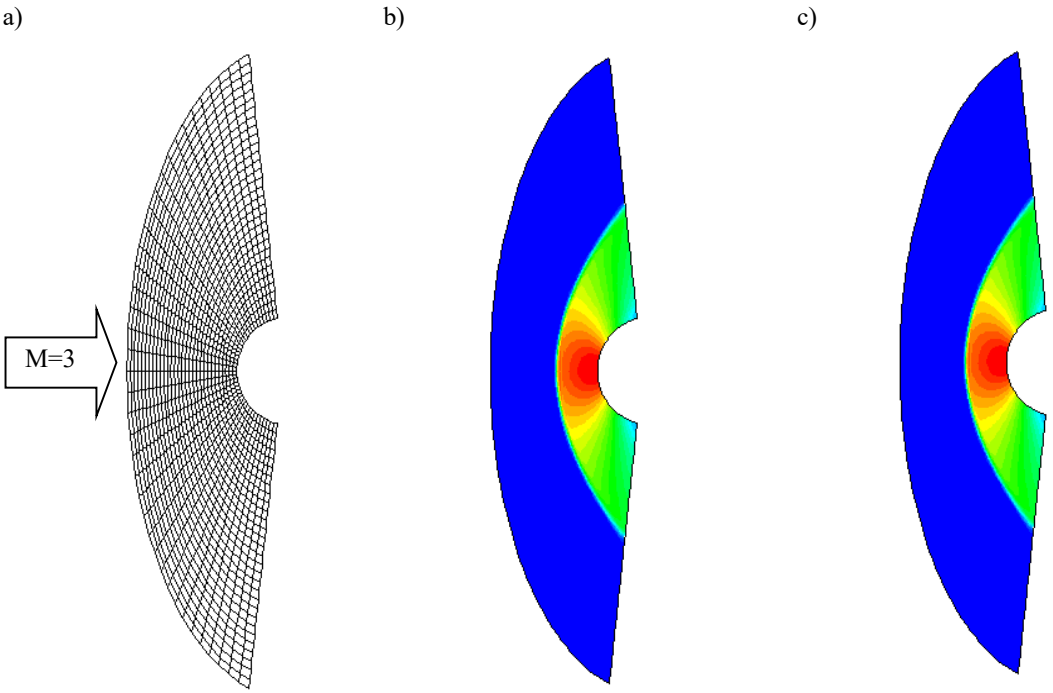

Fig. 12 Supersonic Flow past Cylinder, a) grid, b) HLLCL, and c) HLLCL (θ=1).

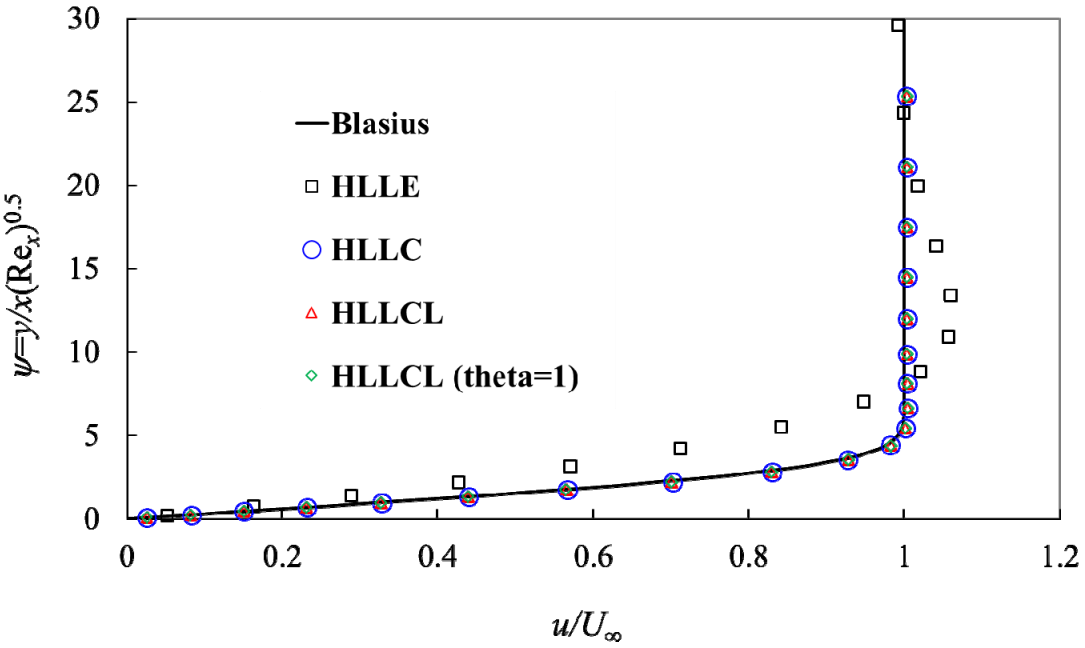

Fig. 13 Mach 0.2 flow over flat plate (velocity profiles at i=30; x= 0.4852E-02).

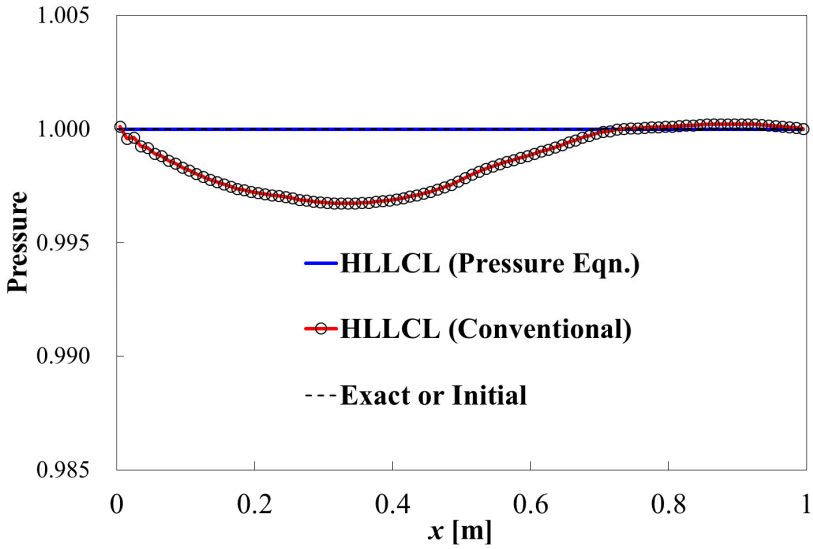

Fig. C.1 Nitrogen Interface Advection Result (HLLCL): pressure, where "Pressure Eqn." stands for the supercritical-fluid-extended version, and "Conventional" is the original HLLCL [19].

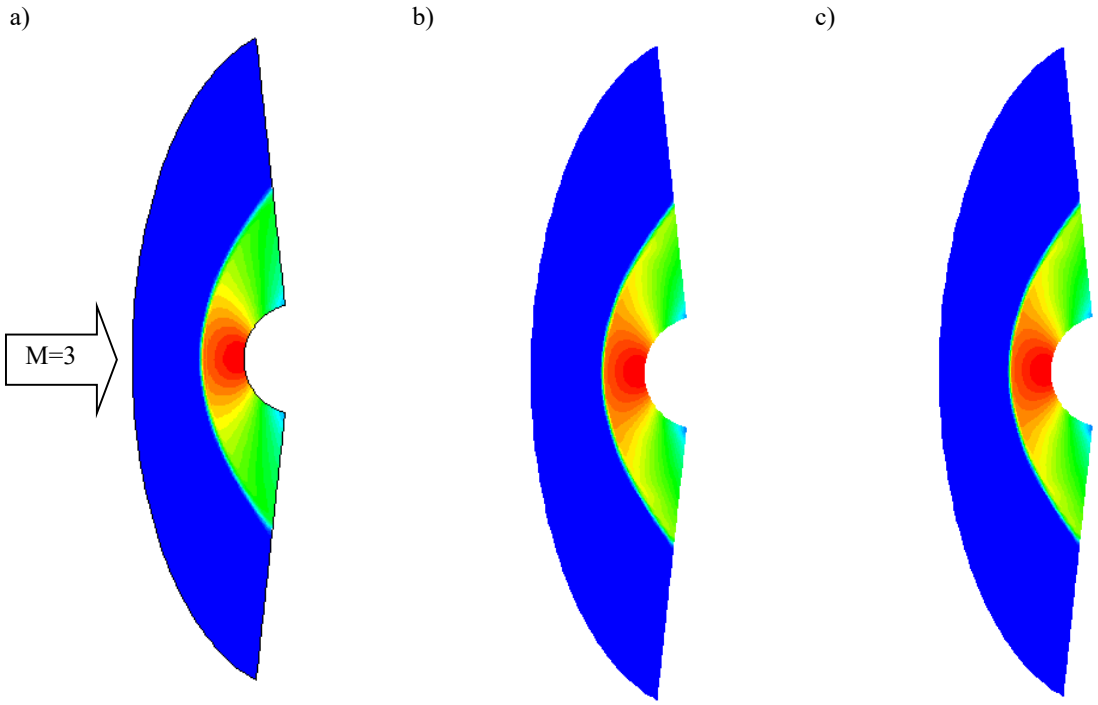

Fig. D.1 Supersonic Flow past Cylinder, a) (k, M_c) = (1, 0.1) (default, Fig.7b), b) (k, M_c) = (1, 1.0), and c) (k, M_c) = (2, 0.1).

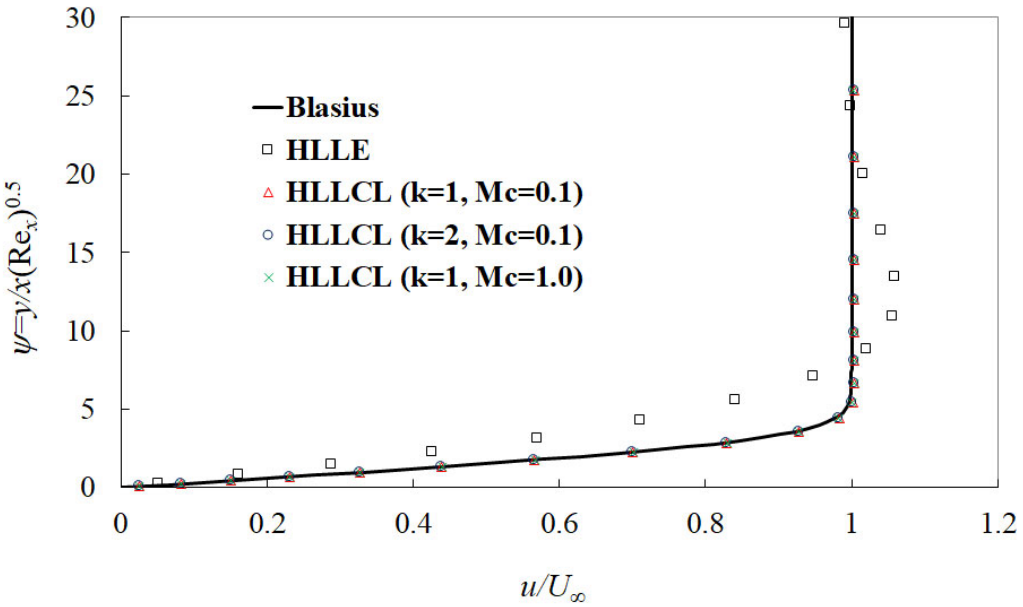

Fig. D.2 Mach 0.2 flow over flat plate (velocity profiles at i=30; x= 0.4852E-02): (k, M_c) = (1, 0.1), (1, 1.0), or (2, 0.1).

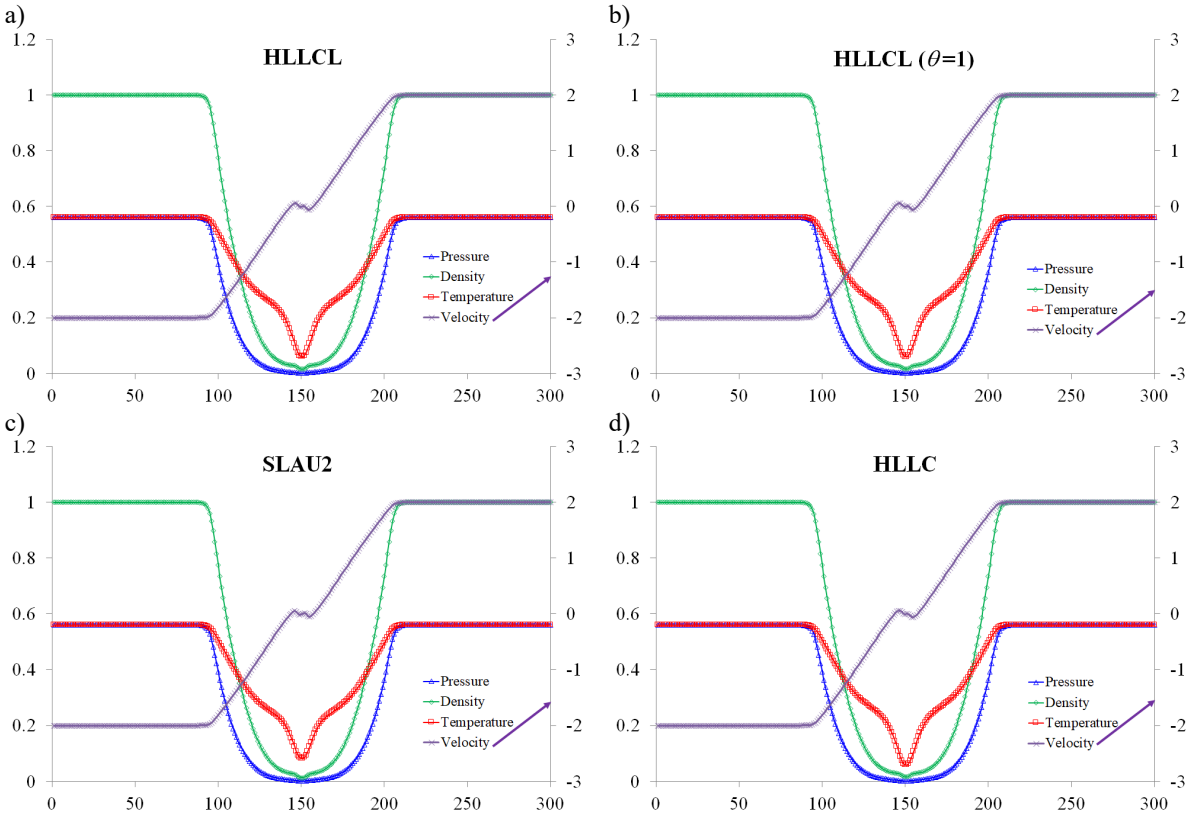

Fig. E.1 Vacuum Problem Solutions, a) HLLCL, b) HLLCL (θ=1), c) SLAU2, and d) HLLC.

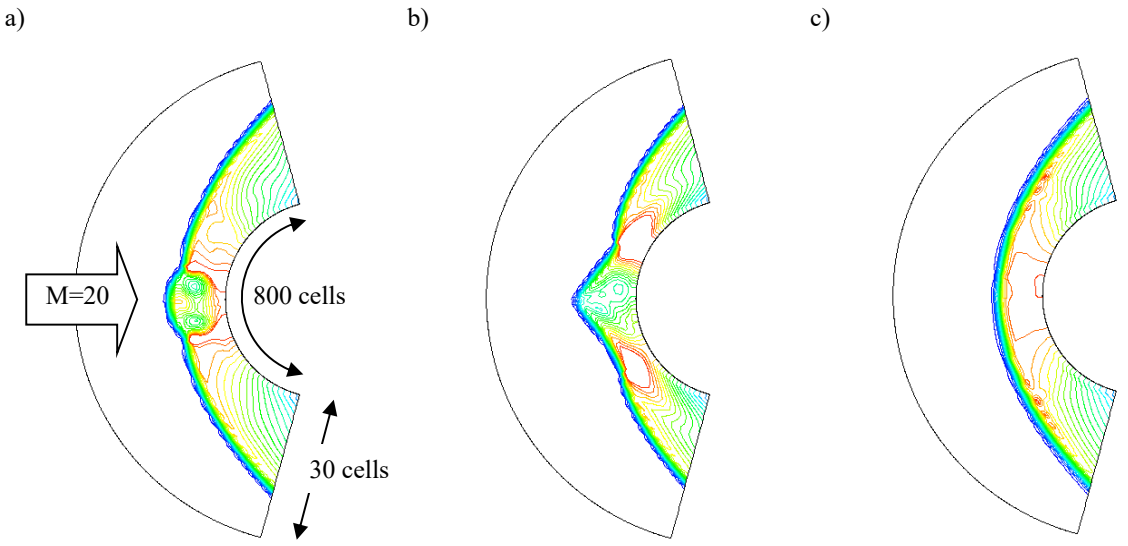

Fig. F.1 Severe Mach 20 with Large-Cell-Aspect-Ratio Problem, a) HLLCL, b) HLLCL (θ=1), and c) SLAU2.